Adsorption isotherms of water in Li–, Na–, and K–montmorillonite by molecular simulation

E. J. M. Hensen,[a] T. J. Tambach, A. Bliek, and B. Smit
Department of Chemical Engineering, University of Amsterdam, Nieuwe Achtergracht 166, 1018 WV Amsterdam, The Netherlands

(Received 5 March 2001; accepted 25 May 2001)

A biased Monte Carlo method for the insertion of water in dense clay–water systems is presented. The use of this algorithm results in a considerable increase of the success rate of insertion attempts. It allows us to compute water adsorption isotherms up to high water densities, where the conventional Monte Carlo scheme fails. The isotherms were calculated by a combination of molecular dynamics and grand-canonical Monte Carlo simulation for Li–, Na–, and K–montmorillonite at a fixed $d(001)$ spacing of 12.0 Å. At low water pressure, the degree of clay hydration is governed by the type of counterion, Li–montmorillonite having the highest water content. Hydrogen bonding between water molecules is absent. Li^+ and Na^+ are small enough to be organized in two layers close to the clay mineral surfaces, whereas K^+ is mainly located in the midplane. In both cases, the water molecules primarily reside in the midplane of the interlayer. Increasing the water pressure leads to water adsorption at higher energy sites closer to the surface, i.e., coordinating to the structural OH groups in the hexagonal cavities. A hydrogen bond network is formed in the clay interlayer. This points to water condensation and leads to a sharp increase in the clay water content. © *2001 American Institute of Physics.* [DOI: 10.1063/1.1386432]

I. INTRODUCTION

Swelling 2:1 clay minerals play an important role in a number of engineering, environmental, and petrological processes. These clays consist of negatively charged silicate layers. The negative charges are compensated by interlayer counterions. These counterions and the charged clay mineral surfaces interact strongly with polar solvents, most notably water. This results in the well-known swelling of smectites and vermiculites. Clay swelling in solids leads to the adsorption of organic molecules and exchange of cations, processes that are of environmental concern. Moreover, the unwanted swelling of clay-rich shales causes bore-hole stability problems which in extreme cases can lead to well-bore collapse during oil exploration.[1] The swelling properties of clay minerals are exploited in applications as adsorbent, ion exchanger, and molecular sieve catalyst.[2]

The interlayer swelling of smectite minerals such as montmorillonite proceeds stepwise through the formation of one-, two-, and three-layer hydrates. The equilibrium water density of such a hydrated clay depends on the type of clay mineral, the type of interlayer counterion, the applied pressure and temperature, and the water vapor pressure.[3–6] Although clay swelling is well understood on a qualitative level, the quantitative details are difficult to access experimentally, especially on the molecular level. Statistical-mechanical computer simulations are ideally suited to obtain such microscopic insight. Especially, the molecular structure of water and the distribution of counterion species in the interlayer have been topics widely addressed by molecular dynamics and Monte Carlo methodologies.[7–15] Several interaction potentials have been used such as the *ab initio*-based MCY model,[7–12,14] the TIP4P model,[11,13] and the SPC/E model.[15] Generally, the results from these studies are qualitatively in fair agreement. Reviews on such molecular simulations are available.[16,17]

In most clay applications, the system is open with respect to water transport. An example is the measurement of water adsorption isotherms in clay minerals.[18] Most simulations have been performed in the constant NVT ensemble, although grand-canonical (GC) ensemble simulations are the preferred method. These latter simulations have been difficult to apply since the probability of acceptance of insertion/removal attempts in the geometrically confined and dense clay–water system is generally low, thereby making such studies expensive. Skipper *et al.*[7,9] and more recently Young and Smith[15] circumvented this problem by performing simulations in the constant NpT ensemble, i.e., by applying constant stress on the clay layers and allowing volume changes at a given water content. A drawback of this method is that it cannot predict the clay water content. GC simulations have been performed in the past by several authors at a fixed interlayer spacing.[19–21] For instance, Karaborni *et al.*[20] used the minima in disjoining pressure as a function of the interlayer spacing calculated from a series of constant μVT simulations to determine the stable states of Na–montmorillonite. They employed a combination of molecular dynamics and Monte Carlo techniques. In essence, this represents the experimental situation of the surface-force-apparatus, where the force perpendicularly on the clay layers is measured while increasing the water vapor pressure. Although this is not representative for most clay applications, these calculations show interesting details on the way water is bonded to

[a]Electronic mail: hensen@its.chem.uva.nl

the different clay constituents and how the water structure is developed. These simulations were limited to one particular cation (Na^+) and one chemical potential ($\mu=-42.8$ kJ mol^{-1}). The type of counterion plays an essential role in the hydration of these clay minerals. Therefore, we extend this study to include other counterions (Li^+ and K^+). The water density in hydrated clays widely varies between the various simulations presented in the literature as outlined by Bleam.[16] These differences may be explained in terms of different water models or different conditions, i.e., temperature and chemical potential of the reservoir that is in contact with the clay. In most petrological applications water is present at elevated pressures. This implies that within the clay the water density can be relatively high.

To perform a successful GC simulation, it is important to successfully insert and remove water molecules into and from the system. At elevated water pressures the conventional GC techniques are not very efficient and in this contribution we develop a biased Monte Carlo technique to increase the success rate of Monte Carlo insertion/removal attempts of water in the hydrated clay. The advantage of this method is that it can be carried out at more reasonable computational cost.

II. METHODS

A. Model

Here, we present combined molecular dynamics and Monte Carlo simulations of water and counterions in a montmorillonite clay. Montmorillonite is a dioctahedral 2:1 clay mineral with the unit-cell formula $M_x^+[Si_8][Al_{4-x}Mg_x]O_{20}(OH)_4$. In the present simulation, M was Li, Na or K and the layer charge x was set to 1.0. The simulation cell contained eight clay unit cells. This results in a clay patch of 21.12×18.28 Å with a thickness of 6.56 Å. The $d(001)$ spacing is taken as 12.00 Å. Three-dimensional periodic boundary conditions, were applied. In order to obviate problems arising from these periodic boundary conditions we used a cutoff radius of 9.14 Å in the nearest-image convention for short-range interaction by duplicating the cell in the direction of the *c*-axis.The long-range Coulomb interactions in the system were treated with the Ewald summation method with a reciprocal space cutoff ($k<3$ Å^{-1}). The time step of the MD simulations was 1 fs. A snapshot of part of the simulation cell is depicted in Fig. 1.

The interaction model for the water–clay interactions (SRM28) is the one developed by Skipper *et al.*[7] and is based on the *ab initio* MCY model for water.[22] The clay layers are kept rigid, while the water and counterions are allowed to move during the MD simulation. The cation–clay and cation–water interaction potentials for Li^+, Na^+, and K^+ are taken from Skipper *et al.*[7] and Park and Sposito.[23] The MCY model was used for the water–water interactions. Water bond constraints (O–H and H–H distances) were enforced by the Shake algorithm.

B. Simulations

The simulations with variable water content were performed in the GC ensemble. The temperature of the water reservoir was fixed at 298 K. A large range in water pressures was covered by varying the chemical potential of this reservoir. A known problem of the MCY model relates to the high pressure needed to maintain liquid water at a density of 1 g cm^{-3} at 298 K.[24] Therefore, the water fugacity was expressed relative to the saturated water vapor pressure. The liquid coexistence density of MCY water at 298 K was estimated by a zero pressure simulation[25] and the corresponding chemical potential was found to be $\mu_L=-37$ kJ mol^{-1}.

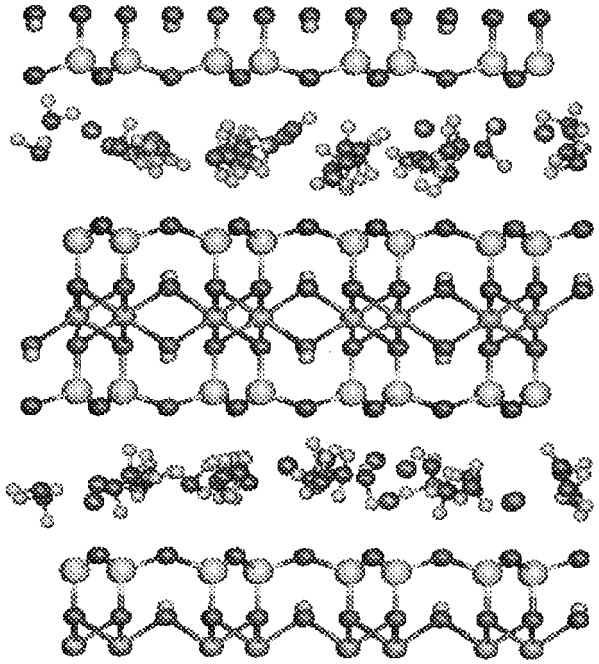

FIG. 1. Equilibrated configuration of a Na–montmorillonite system with $H_2O/Na^+=3$. The $d(001)$ spacing is 12.0 Å. The simulation cell is repeated periodically in all directions. The systems contains two clay sheets, sixteen sodium ions, and interlayer water.

We employ several Monte Carlo sampling schemes to insert and remove water molecules that are described in more detail in Sec. II C. Combined Monte Carlo and molecular dynamics were started with 32 water molecules and 16 ions that were randomly placed in the interlayer region. Constructing the adsorption isotherm was carried out by starting a simulation at a certain water pressure with an equilibrium configuration expediting from a lower water pressure simulation. Initially, the particles were allowed to move for a 10 ps trajectory while scaling their velocities to a temperature of 298 K at each time step. Subsequently, a Nosé–Hoover thermostate[26,27] was applied at a temperature of 298 K. A typical GCMC-MD run included a molecular dynamics simulation with Monte Carlo attempts to insert or delete a water molecule each third MD time step. Statistical averages (oxygen, hydrogen, and counterion density profiles, angle and radial distribution functions) were derived at several water fugacities.

C. Biased Monte Carlo scheme

Monte Carlo algorithms can be biased in order to increase the probability of acceptance.[25] In our simulations we bias the insertion/deletion of water molecules. Similar methods have been applied, for example, to the insertion of alkanes in zeolites[28] and of water molecules in liquid water.[29]

In the case of aqueous systems at high density, it is difficult to find nonoverlapping positions resulting in low acceptance ratios for insertion. Also, the relative molecular orientation has to be acceptable, since water is a strong hydrogen-bond former. The constrained geometry between the clay layers forms an additional difficulty. It is our aim to increase the probability of finding nonoverlapping conformations with acceptable orientation at reasonable computational cost. The insertion of alkanes in zeolites, a problem similar in nature, was addressed by trying many positions to place the first atom of the alkane chain.[30] Similarly, we try to first find an acceptable place for the oxygen atom of a water molecule to be inserted. Therefore, we place many ''first'' oxygen atoms (multiple first beads) and choose the most favorable one. Only, the short-range part of the potential energy is calculated, since this is inexpensive while providing a good indication of the suitability of the trial positions. Normally, when molecules are inserted in one step the total potential is calculated. However, it is equally permitted to use part of the potential in a biased Monte Carlo scheme as long as the necessary corrections are applied to the acceptance rule. This is more extensively outlined in Ref. 25. In the next step, the hydrogen atoms are placed around the selected oxygen atom in several random orientations corresponding to the constraints imposed by the MCY model. Again, we only calculate the short-range components of the potential energy. For this purpose, the MCY model is suited, since short-range potentials are assigned to the hydrogen atoms in contrast to most other water models. The most favorable conformation is selected. The probability that a particular conformation is generated is the product of the probabilities of the first oxygen to be selected and the hydrogen atoms to be selected and increases with the number of trial attempts. Finally, the expensive Coulomb energy is calculated for the selected configuration and the acceptance rule is changed to satisfy detailed balance.[25]

We employ the following scheme for the trial insertion of a water molecule:

Step 1: In inserting a new water molecule, k_O trial positions for the oxygen atom are generated in the simulation cell. We calculate for each position the short-range (SR) component of the potential energy $u_{SR}^{O}(m_i)$ with all other atoms within the real space cutoff radius. We define the Rosenbluth factor,

$$W_O = \sum_{m_i=1}^{k_O} \exp[-\beta . u_{SR}^{O}(m_i)], \tag{1}$$

where $\beta = 1/k_B T$, and select out of the k_O trial positions one atom where each atom m_i has the probability,

$$p(m_i) = \frac{\exp[-\beta . u_{SR}^{O}(m_i)]}{W_O}. \tag{2}$$

Step 2: Next, we generate k_H trial conformations of the hydrogen atoms around the selected oxygen atom with the geometry imposed by the MCY model. The short-range component of the potential energy $u_{SR}^{H}(n_i)$ for these hydrogen atoms is also calculated. This contributes to the Rosenbluth factor,

$$W_H = \sum_{n_i=1}^{k_H} \exp[-\beta . u_{SR}^{H}(n_i)], \tag{3}$$

and out of these k_H conformations we select one, where each conformation has the probability,

$$p(n_i) = \frac{\exp[-\beta . u_{SR}^{H}(n_i)]}{W_H}. \tag{4}$$

Step 3: In step 1 and 2 we have generated an acceptable position and orientation of the water molecule using only part of the total potential. In this step we compute the remainder of the potential with the selected position (1) and orientation (2), i.e., the real (u_C^{real}) and reciprocal (u_C^{recpr}) space part of the Coulomb potential. This last part can be efficiently calculated, when one stores the intermediate results during the energy calculation of the last MD step. It is important to note that this part of the calculation is only performed for a single configuration of the water molecule.

The insertion attempt is accepted with a probability,

$$P_{acc}(N \to N+1) = \min\left[1, \frac{V}{\Lambda^3 (N+1)} \frac{W_O}{k_O} \frac{W_H}{k_H} \times \exp[\beta(\mu - u_C^{real} - u_C^{recpr})]\right], \tag{5}$$

where N is the number of water molecules of the initial configuration, V is the total volume of the simulation cell, and Λ is the thermal de Broglie wavelength.

For the removal of a water molecule we have to compute the Rosenbluth factor of the oxygen, W_O, and the hydrogen atoms, W_H, of the selected molecule. For W_O we use step 1 of the previous algorithm except that we generate only $k_O - 1$ positions plus the position of the oxygen atom of the selected configuration. For the Rosenbluth factor of the hydrogen atoms, W_H, similar to step 2, $k_H - 1$ conformations are generated and these plus the conformation of the hydrogen atoms of the selected water molecule determine W_H. The acceptance rule for the removal of a water molecule becomes

$$P_{acc}(N \to N-1) = \min\left[1, \frac{\Lambda^3 (N+1)}{V} \frac{k_O}{W_O} \frac{k_H}{W_H} \times \exp[\beta(-\mu + u_C^{real} + u_C^{recpr})]\right]. \tag{6}$$

The expensive calculation of the Coulomb energy is only performed for a configuration that has a reasonable chance of being accepted. Besides the described Monte Carlo scheme (denoted as multiple first bead−1, MFB-1), we also designed a scheme (MFB-2) that consisted of inserting the water molecule in three steps: (i) insertion of an oxygen atom (k_O attempts), (ii) the insertion of the first hydrogen atom randomly (k_{H1} attempts) and (iii) the insertion of the second hydrogen atom randomly at the correct HOH angle (k_{H2}). AM (all molecule) refers to the method where the entire water molecule is inserted without biasing methods. For the calculation of the water adsorption isotherms we used the MFB-2 method with $k_O = 10$, $k_{H1} = 25$, and $k_{H2} = 25$.

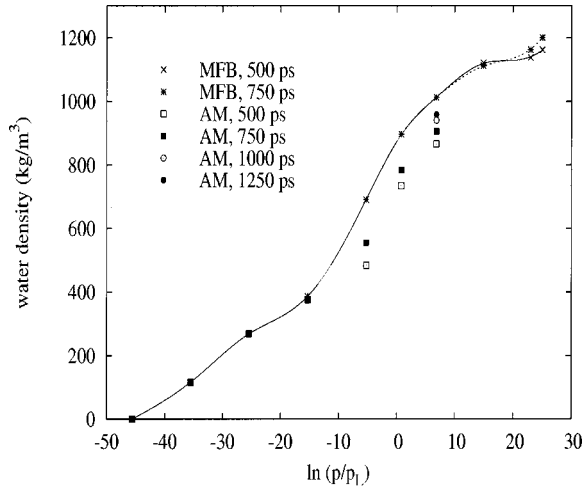

FIG. 2. The water density as a function of the water fugacity for Na–montmorillonite computed by different methods and simulation times.

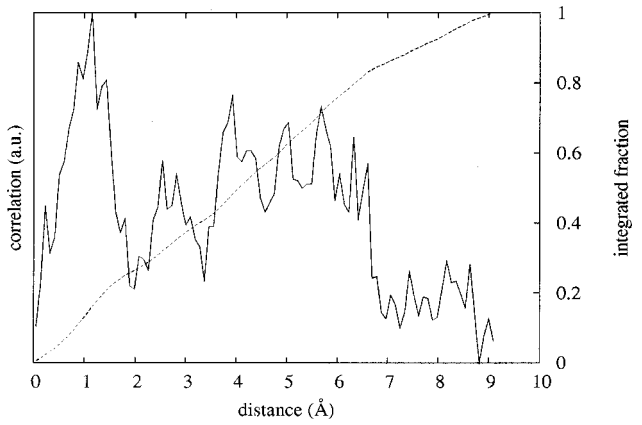

FIG. 3. Correlation between the position of a deleted water molecule (origin) and a subsequently inserted water molecule (left, full line) and the integrated fraction of insertions (right, dashed line) at a density of 400 kg/m^3.

Since the SRM28 model uses no short-range contributions to the potential of the atoms in the middle of the clay sheets, this leads to the incorrect insertion of water molecules within the clay sheets. To avoid this, dummy particles were added in the middle plane of the clay layers in the GCMC-MD simulations. The interaction potential for these particles was chosen such that their contribution to the potential in the interlayer region was negligible.

D. Evaluation of methods

The computational efficiency of the biased Monte Carlo methods is exemplified in Fig. 2. It shows the computed water densities for Na–montmorillonite as a function of the water fugacity obtained by the AM method and the MFB-2 method after several simulation times. As we will discuss later the use of the MFB-2 method increases the CPU time by 10%–20%. For an infinite amount of CPU time both methods should give identical results. The results obtained from the MFB method are equilibrium water densities. This is judged from the equivalence of the number of successful insertion and removal attempts, provided that this number is significantly high (at least 500). Moreover, the extended simulation of 750 ps reproduced the water densities up to high water pressure. However, success rates become very low due to the high density at high water pressure and longer simulations are needed to ensure sufficient sampling. An alternative to extending the simulation is to increase the number of trial attempts (k_O and k_H) of the biased scheme.

One point of concern relates to the insertion of water molecules near positions where recently a water molecule has been deleted. This means that we obtain a high probability of inserting new molecules but that no statistically independent configurations are generated. This leads to inefficient sampling of the clay water content. To ensure that this is not the case, we calculated the correlation between the position of removal of a water molecule and a subsequent insertion. The resulting correlation function of the distance between removal and a subsequent insertion and the integrated fraction is shown in Fig. 3. If the insertions would be completely correlated we would observe a single peak around 0 Å. The peak at 1 Å indicates that some correlation exists but most of the molecules are inserted sufficiently far away from the previously deleted molecules.

The probability of a successful insertion in the simulation cell is the product of the probabilities of the occurrence of a density fluctuation permitting an insertion, of finding this fluctuation and generating an acceptable orientation. Obviously, the biased Monte Carlo scheme aims to increase the latter two probabilities. The computational efficiency is evaluated by determining the acceptance probability for a number of trial insertions of water in a configuration, where such a density fluctuation is present. Tables I and II show the acceptance probability (P_{acc}) and the associated CPU time (τ) for medium and high density, respectively. Note that the CPU time for one Monte Carlo insertion attempt (unbiased scheme-AM) represents 20% of the CPU time needed for

TABLE I. The acceptance probability of water insertion in cation-exchanged montmorillonite (medium water density =500 kg/m^3) and the associated CPU time as a function of the Monte Carlo method (AM=all molecule, MFB=multiple first beads, and k=the number of trial positions). N_{acc} is the number of attempts, Acc. is the percentage of accepted attempts, τ is the CPU time for the MC algorithm relative to the one for the unbiased method.

	N_{acc}	k_O	k_H	k_H	Acc.(%)	τ
AM	10^6	⋯	⋯	⋯	0.02	1
MFB-1	10^6	1	1	⋯	0.02	1.0
	10^6	1	5	⋯	0.04	1.1
	2.10^5	5	1	⋯	0.06	1.1
	10^5	10	1	⋯	0.09	1.2
	4.10^4	25	1	⋯	0.13	1.4
	10^5	10	10	⋯	0.14	1.5
	10^5	10	25	⋯	0.14	2.0
	2.10^4	50	25	⋯	0.23	2.7
MFB-2	10^6	1	1	1	0.02	1.0
	10^6	1	5	1	0.03	1.1
	10^6	1	1	5	0.03	1.1
	2.10^5	5	1	1	0.06	1.1
	2.10^5	5	5	5	0.09	1.2
	10^5	10	10	10	0.11	1.4
	10^5	10	25	25	0.11	1.7
	4.10^4	25	25	25	0.20	1.7

TABLE II. The acceptance probability of water insertion in cation-exchanged montmorillonite (high water density=900 kg/m^3) and the associated CPU time. For further information, the reader is referred to Table I.

	N	k_O	k_H	k_H	Acc.(%)	τ
AM	10^6	⋯	⋯	⋯	0.004	1
MFB-1	10^6	1	1	⋯	0.004	1.0
	10^5	10	10	⋯	0.06	1.2
	4.10^4	25	25	⋯	0.13	1.8
	2.10^5	50	25	⋯	0.21	2.1
MFB-2	10^6	1	1	1	0.004	1.0
	2.10^5	5	5	5	0.03	1.2
	10^5	10	10	10	0.05	1.3
	10^5	10	25	25	0.05	1.5
	4.10^4	25	25	25	0.09	1.8
	2.10^4	50	50	50	0.13	2.5

one molecular dynamics step. P_{acc} for the biased methods with $k_O=1$ and $k_H=1$ correspond to the value obtained by the AM method. The acceptance probability strongly increases when more oxygen positions (k_O) are attempted. P_{acc} can be increased further by allowing more hydrogen atom(s) conformations. This is computationally very efficient, since it is advantageous to try to find a reasonable hydrogen conformation after finding a suitable oxygen position. The computational cost for these methods is low. For instance, increases in P_{acc} of a factor of 10 are obtained, while τ only increases by a factor of 3. This efficiency largely stems from the advantage of having to calculate the Coulomb energy by the Ewald summation only once. In the case of the unbiased AM method, this last calculation constitutes over 90% of the total CPU time for a trial insertion. Comparing the MFB-1 and -2 method, one observes that the MFB-1 method is the preferred one. This relates to the constrained conformation of the hydrogen atoms. Suitable conformations are more efficiently sampled when both hydrogen atoms are placed at once. Comparing the results at medium and high density, it follows that the acceptance probability of the AM method at high density becomes very low due to the low probability of finding nonoverlapping oxygen positions. However, also in this case the biased methods can efficiently increase P_{acc}.

Overall, the number of successful insertion/removal attempts decreases at higher density because the probability that a density fluctuation occurs becomes smaller. While we performed MC attempts each third MD time step in the present simulations, this may be increased to, for instance, each time step to increase the probability of finding these fluctuations.

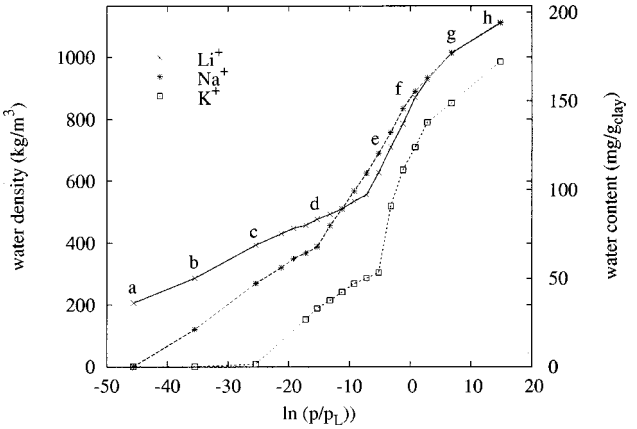

FIG. 4. The water density (left) and clay water content (right) as a function of the water fugacity for Li–, Na–, and K–montmorillonite computed by the MFB method.

In essence, the relation between clay water content and water fugacity represents the water adsorption isotherm for Na–montmorillonite at a fixed $d(001)$ spacing of 12 Å. The AM method reproduces this adsorption isotherm at low, but fails to do so at higher water fugacity. These deviations become smaller by extending the simulation to 750 ps, but results obtained from even longer simulations (1000 and 1250 ps) at $\ln(p/p_L)\approx 8$ show that simulation times to reach equilibrium become unrealistically high. One concludes that P_{acc} in the conventional scheme is too low making the computation of water adsorption isotherms in clay systems prohibited. The use of multiple first beads methods leads to a significant increase of the acceptance probability of insertion/removal attempts. This enables us to determine water adsorption isotherms up to very high water densities. These high water densities relate to situations of high water pressure.

III. RESULTS AND DISCUSSION

The water adsorption isotherms for Li–, Na–, and K–montmorillonite are presented in Fig. 4. These data show that the influence of the type of exchangeable counterion is

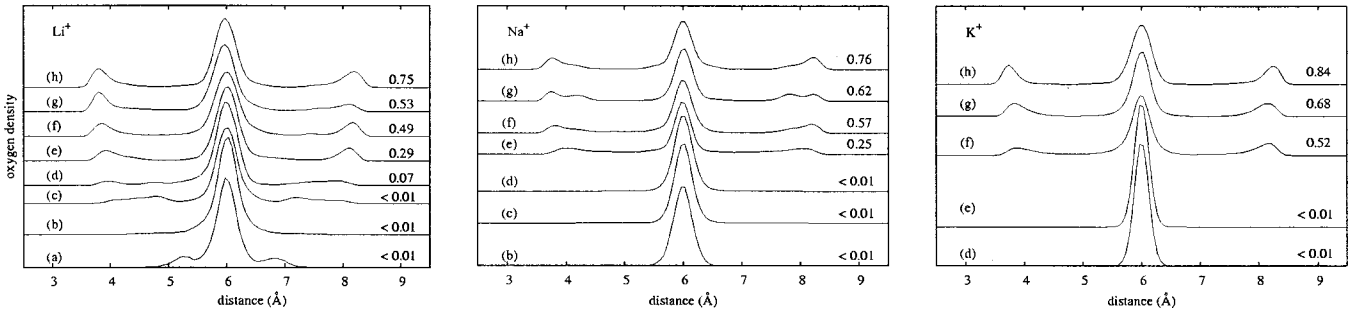

FIG. 5. Oxygen density profiles for Li–, Na–, and K–montmorillonite. The values at the right indicate the computed hydrogen bond index (a–h correspond to the fugacities in Fig. 4).

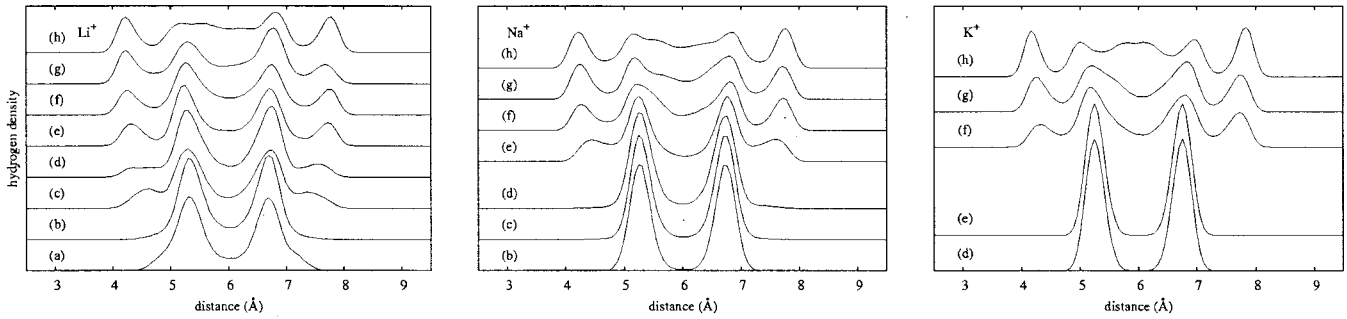

FIG. 6. Hydrogen density profiles for Li–, Na–, and K–montmorillonite (a–h correspond to the fugacities in Fig. 4).

paramount at low water fugacity. In this regime, the hydration of the clay shows the following well-known order: $Li^+ > Na^+ > K^+$. These differences are explained on the basis of the cation hydration energy that decreases from the small Li^+ to the larger K^+. Figure 5 depicts the corresponding oxygen density profiles in the direction perpendicular to the clay layers. The hydrogen bond index is also indicated. This value represents the average number of hydrogen bonds per water molecule and is therefore a measure for the hydrogen bonding network formed between the clay layers. Here, we adopt the definition of Ferrario *et al.*,[31] i.e., two molecules are hydrogen-bonded if simultaneously the interoxygen distance is less than 3.5 Å and the O–HO angle is smaller than 30°. Note that a separate simulation of bulk MCY water (64 molecules, density=996 kg/m^3) gave a value of 1.51 for the hydrogen bond index.

The very low hydrogen bond index (index <0.01) implies that the water molecules do not form hydrogen bonds. At low water fugacity, the water oxygen atoms are preferentially situated in the midplane of the interlayer. The hydrogen density profiles (Fig. 6) indicate that the water molecules are either oriented with their hydrogen atoms to the same clay sheet as also indicated by neutron-diffraction experiments on Na–vermiculite[32] (a high charge clay with mainly tetrahedral substitution) or with their dipole vectors parallel to the clay mineral surfaces and the hydroxyl groups directed toward each of the latter. Figure 7 shows the distribution of the angle between the water dipole vector and the normal to the nearest

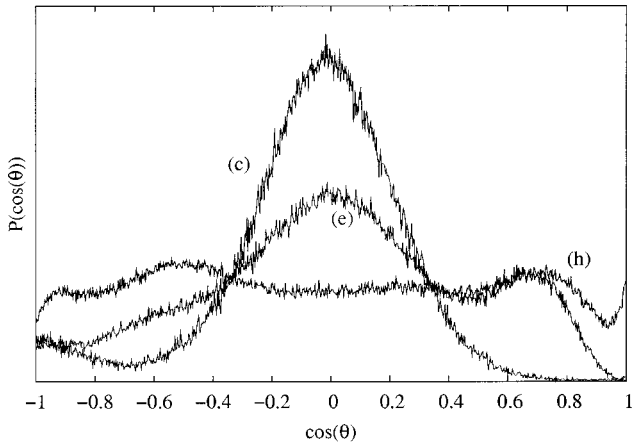

FIG. 7. Angle distribution (water dipole vector with clay normal) for Na–montmorillonite at various water contents.

clay mineral surface for Na–montmorillonite. This shows that the second assertion is in line with our simulation. It corroborates with earlier computer simulations by Chang *et al.*[10] This preferential orientation does not allow hydrogen bonds to be formed. The counterion density profiles in Fig. 8 point to an essential difference between Li^+ and Na^+ on the one hand and K^+ on the other. The smaller counterions are organized in two layers close to the surface, whereas the larger K^+ essentially forms a monolayer in the midplane. The Li^+ density profile shows that its mobility normal to the clay layers is strongly hindered. Na^+ shows a similar behavior, but its adsorption to the clay layers appears to be less strong (Li^+ is approximately 0.2 Å closer to the siloxane surface). Moreover, there is considerable Na^+ density in the midplane also pointing to a higher mobility. A more detailed structural analysis shows that at these low H_2O/counterion ratios the water molecules are sometimes shared between several counterions next to counterions that form bonds with free water molecules. In the case of K^+, the water molecules reside in the same plane as the counterions. For Na^- and Li^- montmorillonite, the water molecules are mainly in the midplane coordinating to the counterions that are located closer to the clay mineral surface. Particularly for the small and strongly coordinating Li^+, we observe that water molecules sometimes leave the midplane and coordinate to the structural OH groups. This explains the small, but significant oxygen density closer to the clay mineral surface at low water fugacity. One important approximation of the present calculations relates to the use of effective pair potentials for the counterion–water interactions. In practice, the hydration energy is higher for incompletely solvated cations as encountered at low water fugacity, while the use of effective pair potentials imposes a mean value for the hydration energy. Nevertheless, these potentials enable us to discriminate between the extent of hydration of clays with various counterions.

We observe a sharp increase in the clay water content for all three types of clays at a certain water fugacity. The oxygen density profiles indicate that the extra water molecules are located near the siloxane surface. These sites represent a higher energy than the sites in the midplane. Figure 7 shows that these water molecules are oriented with their hydrogen atoms into the interlayer and a more detailed analysis shows that these water molecules coordinate with their oxygen atom to the structural OH groups in the hexagonal cavities.

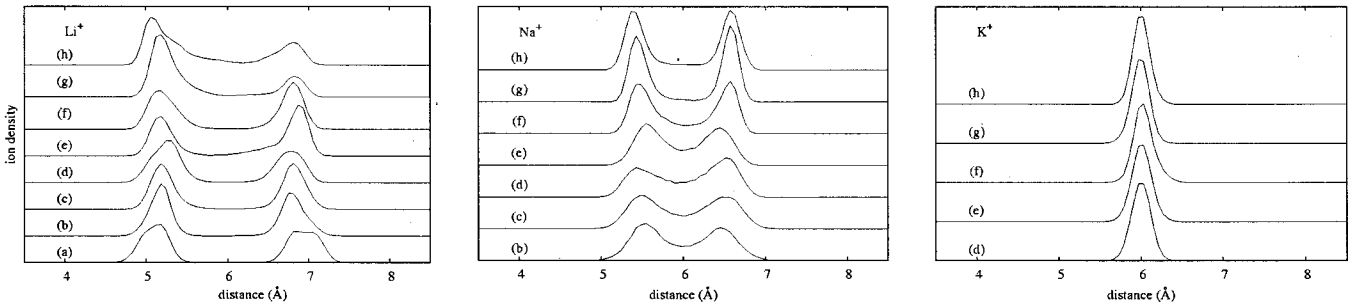

FIG. 8. Counterion density profiles for Li–, Na–, and K–montmorillonite (a–h correspond to the fugacities in Fig. 4).

This water configuration has been described before in simulation[20,33] and experiment.[32] It appears that the dipole vector of these water molecules is not perpendicular to the clay surface but slightly tilted. This is due to the competition between coordination to the counterion and the formation of hydrogen bonds with siloxane oxygen atoms on the one and the structural OH group on the other hand. Concomitant with water adsorption at these sites, the hydrogen bond indices sharply increase for all three types of clay. A more extensive hydrogen bonding network is formed, although the values are below the value of the bulk. This partly stems from not taking into account the bonding of water molecules to the siloxane surface. These findings strongly point to condensation of water in the interlayer. Although we did not calculate the desorption isotherm by starting from high clay water content, we expect that the transition to lower water density occurs at lower chemical potential in line with experimentally observed hysteresis.[34,35] For Li– and K–montmorillonite this transition is observed at $\ln(p/p_L) \approx -5$, while the increase in clay water content of their Na–montmorillonite occurs at lower chemical potential. The reason for this most probably relates to the fact that the fixed $d(001)$ spacing is the equilibrium spacing for Na–montmorillonite,[20] but not for the other two clays.[11,12] This allows a more efficient packing of the water molecules and water condensation at lower water fugacity for Na–montmorillonite. Strikingly, the water content in K–montmorillonite remains lower than in its Na- and Li-counterparts at high water fugacity. Furthermore, the water content of the latter two clays is approximately equal in this regime. The organization of Na^+ and Li^+ in two layers closer to the surface allows more water molecules to be adsorbed in the energetically favorable midplane. This contrasts to the situation for K–montmorillonite, where less water molecules can be adsorbed due to the presence of the counterion in the midplane.

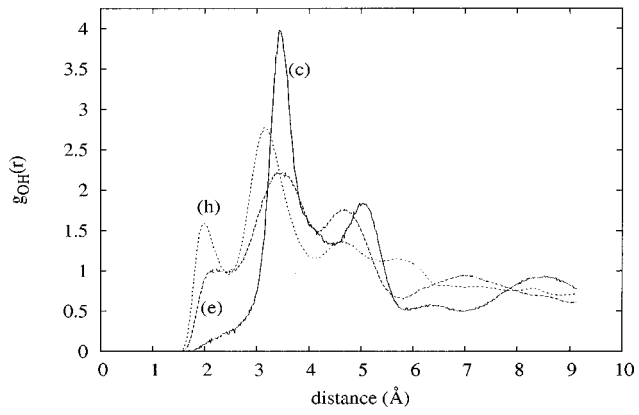

FIG. 9. OH radial distribution function for Na–montmorillonite at various water contents (OH bonds within the water molecule and clay oxygens are not taken into account).

The evolution of the hydrogen bond network is accentuated by the OH radial distribution function for Na–montmorillonite at low, medium, and high clay water content (Fig. 9). The trend is representative for all three types of clay. Note that the differences in maxima and minima in part reflect the difference in water density as outlined by Park and Sposito.[23] The OH peak at 2.0 Å observed at high water fugacity is in line with results by Chang *et al.*[10] Essentially, the absence of the peak at 2.0 Å at low water fugacity shows that no hydrogen bonds are formed between the water molecules. All water molecules mainly reside in the midplane coordinating to the counterions. Such hydrogen bonds are only formed when water molecules are adsorbed at high energy sites near the clay surface.

The present results are to be compared to the results obtained by the groups of Skipper and Sposito that were reviewed by Chang *et al.*[16] The calculated $d(001)$ spacing of the monolayer hydrates in these studies was close to 12 Å using a constant stress in the *c*-axis direction of 10^5 Pa, while the interlayer water densities are in the range of 400–500 kg/m^3. Note that in these studies Wyoming-type montmorillonite with a lower charge ($x=0.75$) containing both tetrahedral and octahedral substitution sites were generally used. Our findings for the structure in this density range agree well with their results, most notably the formation of the small counterions in a bilayer, the preference of water molecule to be adsorbed in the midplane and the coordination of some water molecules to the structural OH groups. The oxygen density profiles of Na–montmorillonite in the present study show less fine structure than the ones calculated by Karaborni *et al.*[20] They also found preferred water adsorption in the midplane, but this was associated with three distinct maxima. Relevant differences with the present study are the absence of the calculation of long-range Coulomb interactions and the inclusion of the flexible OH bonds and HOH bending for the water molecules. Especially, this latter aspect

might be important and the use of flexible water models must be considered in future studies.

Although the present calculations were performed at constant $d(001)$ spacing, the results strongly point to a picture where water adsorption takes place in two distinct steps. A first step is the formation of a hydration shell of the counterions at low water pressure. This is followed by a second step where the remainder of the interlayer volume is filled by adsorption of water molecules coordinating to the clay. An additional driving force for this latter step is the formation of a hydrogen bonding network. Such a mechanism for clay water adsorption has been suggested before.[5,36] An interesting question remains which step leads to crystalline clay swelling and to this end simulations in the μpT ensemble are necessary.

IV. CONCLUSIONS

A biased Monte Carlo method for the insertion of water into the dense clay–water system is presented. The use of a multiple first beads method increases the acceptance probability of the insertion of water at reasonable computational cost. In consequence, it appears possible to perform grand-canonical ensemble simulations at relatively high water density in the geometrically constrained and densely filled clay interlayers. This is a valuable tool to study crystalline clay swelling.

The water adsorption isotherms at a fixed $d(001)$ spacing of 12.0 Å were calculated for Li–, Na–, and K–montmorillonite. Water adsorption in these montmorillonites takes place by two processes. At low water fugacity, adsorption is driven by the hydration of the interlayer counterions. The extent of water adsorption increases with cation–water hydration energy ($Li^+ > Na^+ > K^+$). Although counterion hydration is the main driving force for the adsorption of water, the configuration of the adsorbed water molecules is also influenced by coordination to the clay surface forcing them to the midplane with their dipole vectors parallel to the clay mineral surface. Secondly, at higher water fugacity water molecules are adsorbed near the clay mineral surface coordinating to the structural OH groups. This allows the formation of an extensive hydrogen bonding network and results in a sharp increase in clay water content with water fugacity. We observe that Li^+ and Na^+ are located in two layers closer to the surface compared to K^+, that primarily resides in the midplane. In the latter case, less water molecules can be adsorbed in the energetically favorable midplane resulting in lower clay water contents.

[1] G. M. Bol and S.-W. Wong, Soc. Pet. Eng., **1992**, 24975.
[2] R. E. Grim, *Applied Clay Mineralogy* (McGraw–Hill, New York, 1960).
[3] P. G. Slade, J. P. Quirk, and K. Norrish, Clays Clay Miner. **39**, 234 (1991).
[4] T. Sato, T. Watanaba, and R. Otsuka, Clays Clay Miner. **40**, 103 (1992).
[5] I. Bérend, J.-M. Cases, M. François, J.-P. Uriat, L. Michot, A. Masion, and F. Thomas, Clays Clay Miner. **43**, 324 (1995).
[6] G. D. Cancela, F. J. Huertas, E. R. Taboada, F. Sánchez-Rasero, and A. H. Laguna, J. Colloid Interface Sci. **185**, 343 (1977).
[7] N. T. Skipper, K. Refson, and J. D. C. McConnell, J. Chem. Phys. **94**, 7434 (1991).
[8] N. T. Skipper, F.-R. C. Chang, and G. Sposito, Clays Clay Miner. **43**, 285 (1995).
[9] N. T. Skipper, G. Sposito, and F.-R. C. Chang, Clays Clay Miner. **43**, 294 (1995).
[10] F.-R. C. Chang, N. T. Skipper, and G. Sposito, Langmuir **11**, 2734 (1995).
[11] F.-R. C. Chang, N. T. Skipper, and G. Sposito, Langmuir **13**, 2074 (1997).
[12] F.-R. C. Chang, N. T. Skipper, and G. Sposito, Langmuir **14**, 1201 (1998).
[13] E. S. Boek, P. V. Coveney, and N. T. Skipper, J. Am. Chem. Soc. **117**, 12608 (1995).
[14] J. A. Greathouse and G. Sposito, J. Phys. Chem. B **102**, 2406 (1998).
[15] D. A. Young and D. E. Smith, J. Phys. Chem. B **104**, 9163 (2000).
[16] W. F. Bleam, Rev. Geophys. **31**, 51 (1993).
[17] F.-R. C. Chang, N. T. Skipper, K. Refson, J. A. Greathouse, and G. Sposito, in *Mineral-Water Interfacial Reactions: Kinetics and Mechanism*, edited by D. L. Sparks and T. J. Grundl (American Chemical Society, Washington, 1999), p. 88.
[18] J. Hagymassy, S. Burnanauer, and R. Sh. Mikhail, J. Colloid Interface Sci. **39**, 485 (1969).
[19] A. Delville, Langmuir **8**, 1796 (1992).
[20] S. Karaborni, B. Smit, W. Heidug, J. Urai, and E. van Oort, Science **271**, 1102 (1996).
[21] R. M. Shroll and D. E. Smith, J. Chem. Phys. **111**, 9025 (1999).
[22] O. Matsuoka, E. Clementi, and M. Yoshimine, J. Chem. Phys. **64**, 1351 (1976).
[23] S.-H. Park and G. Sposito, J. Phys. Chem. B **104**, 4642 (2000).
[24] G. C. Lie, E. Clementi, and M. Yoshimini, J. Chem. Phys. **64**, 2314 (1976).
[25] D. Frenkel and B. Smit, *Understanding Molecular Simulation* (Academic, San Diego, 1996).
[26] S. Nosé, J. Chem. Phys. **81**, 511 (1984).
[27] W. G. Hoover, Phys. Rev. A **31**, 1695 (1985).
[28] D. Frenkel, G. Mooij, and B. Smit, J. Phys.: Condens. Matter **4**, 3053 (1992).
[29] R. F. Cracknell, D. Nicholson, N. G. Pasonage, and H. Evans, Mol. Phys. **71**, 931 (1990).
[30] K. Esselink, L. D. J. C. Loyens, and B. Smit, Phys. Rev. E **51**, 1560 (1995).
[31] M. Ferrario, M. Haugney, I. R. McDonald, and M. L. Klein, J. Chem. Phys. **93**, 5156 (1990).
[32] N. T. Skipper, A. K. Soper, and J. D. C. McConnell, J. Chem. Phys. **94**, 5751 (1991).
[33] N. T. Skipper, K. Refson, and J. D. C. McConnell, Clay Miner. **24**, 411 (1989).
[34] P. Malla and N. Komarneni, *Proceedings of the 9th International Clay Conference, Strasbourg, 1989*, edited by V. C. Farmer and Y. Tardy, Sci. Geol. Mem. **86**, 59, Strasbourg, 1990.
[35] M. Sychev, N. Kostoglod, A. Astrelin, M. Rozwadowski, and E. M. van Oers, Kinet. Katal. **39**, 106 (1998).
[36] J. M. Cases, I. Bérend, M. François, J. P. Uriot, L. J. Michot, and F. Thomas, Clays Clay Miner. **45**, 8 (1997).